COMMISSIONING, INITIAL TESTING AND RESULTS FROM AN EXPERIMENTAL ONE KILOWATT ORGANIC RANKINE CYCLE

Michael Southon[1], Susan Krumdieck[1]

[1]*Department of Mechanical Engineering, University of Canterbury, Private Bag 4800, Christchurch 8041, New Zealand*

[1]michael.southon@pg.canterbury.ac.nz

Keywords: *Experimental Organic Rankine Cycle, ORC, Scroll expander, Power generation from waste heat, Zeotropic mixture, M1.*

ABSTRACT

Organic Rankine Cycle (ORC) systems are capable of utilising low-enthalpy heat sources to generate power. The aim of the Above Ground Geothermal and Allied Technologies (AGGAT) research programme is to develop ORC systems within New Zealand. For the design, component selection and operation of ORC systems, it is important to understand process parameters and component behaviour. An experimental scale ORC system, known as ORC-B, has been built and tested at the University of Canterbury to assist in furthering our knowledge of ORC system design and construction.

This paper presents experimental results from running a 1 kW ORC-B system using HFC-M1 refrigerant, a zeotropic mixture of R245fa and R365mfc as the working fluid under several operating conditions. Hot exhaust combustion products from a 30kW Capstone^{TM} Gas Turbine are used as the heat source and heat is transferred via a thermal oil loop to the working fluid through a plate heat exchanger. A scroll expander magnetically coupled to an AC generator is used for work extraction and energy conversion. A thermodynamic analysis of the component performance is undertaken, factoring in several practical aspects of the system and its design. Details on the applied aspects of obtaining accurate results from an experimental ORC system are included, such as the effect of restriction to the flow path, heat losses, pump motor slippage and measurement uncertainty.

1. INTRODUCTION

1.1 ORC background

Rankine cycle systems are commonly used to generate power from thermal sources. An organic Rankine cycle system utilises a refrigerant as the working fluid to generate power from low temperature heat sources at a higher efficiency than a traditional steam system. A small laboratory scale 1kW ORC system called ORC-B has been built and tested at the University of Canterbury as part of the Above Ground Geothermal and Allied Technologies (AGGAT) research programme. The design, component selection and construction of the ORC-B system is detailed in (David Meyer, 2013)

1.2 Purpose of experiments

The ORC-B system was constructed in 2013 at the University of Canterbury in order to provide a test bench for refrigerant heat exchange and various expander configurations.

In its current configuration, a positive displacement scroll type expander is employed as the work extraction device (Lemort, Quoilin, Cuevas, & Lebrun, 2009). Two plate heat exchangers act as the evaporator and condenser, and a positive displacement pump circulates the working fluid.

In intended future work, the test bench will be used to test novel ORC turbine designs.

2. EXPERIMENTAL SETUP

2.1 System

The installed ORC test rig consists of four separate fluid loops – the exhaust gas, thermal oil, refrigerant, and cooling water. These fluids transfer heat to one another through three heat exchangers.

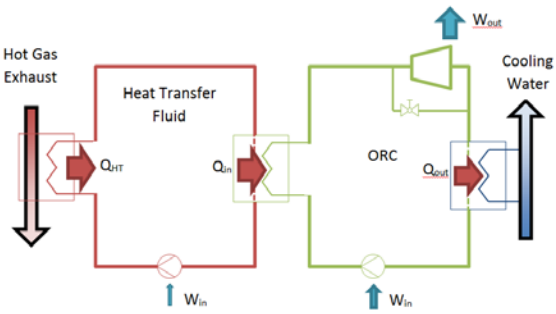

Figure 1: Diagram showing the heat and work flows of the ORC system and thermal oil loop.

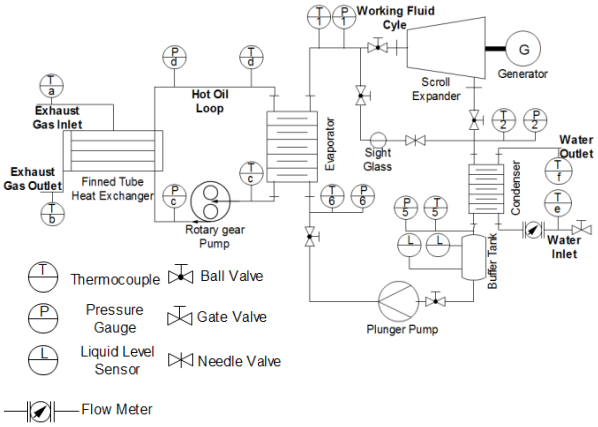

Figure 2: Layout of ORC-B system. Image produced by Leighton Taylor.

2.2 Heat source

A Capstone turbine system is utilized as the heat source for the ORC. The Capstone turbine system combusts diesel fuel, and the hot waste gasses from this combustion are passed through a finned tube heat exchanger (FTHE) to heat the thermal oil in the heat transport loop.

The Capstone turbine is controlled by setting a desired power output between 0 – 30 kW. The flow rate of the gas exhaust products is correlated with this power output setting using manufacturer data (Capstone, 2006). Thermocouples placed inside the gas exhaust stream before and after the FTHE measure the gas temperature drop (Figure 2).

2.3 Heat transport system

As shown in Figure 1, a thermal oil loop is used to transport heat to the ORC system through a plate type heat exchanger, called the evaporator.

The thermal oil is is CALFLOW^{TM} High Temperature Heat Transfer Fluid (HTF) from PETRO-CANADA. Manufacturer data on the density and heat capacity was used for heat rate calculations. The heat capapcity is assumed to be independent of pressure and is given by Equation 1.

$$C_{p,tf} = 3.46 \times T_{tf,m} + 1807.86\ (J/kg) \quad (1)$$

The heat transfer fluid is circulated throughout the thermal oil loop using a gear-type posistive displacement pump. The relationship between pump motor controller speed (set by the user) and the thermal oil flow rate was determined using Equation 2 (Engel, 2013).

$$\dot{V}_{tf} = (0.0103\ L \times n + 0.20\ L/min) \quad (2)$$

Where n is the pump motor controller speed.

The thermal oil loop is insulated and two thermocouples are placed before and after the evaporator to measure the entry and exit temperatures (Figure 2). The thermal oil temperature is assumed to remain constant while flowing in the insultated pipes between the gas and refrigerant heat exchangers.

2.4 ORC system

The ORC system consists of a plate type evaporator, a scroll expander, a plate type condenser, a buffer tank and a working fluid pump (Figure 2).

The working fluid pump is a three-cylinder piston type positive displacement pump controlled through a control box. The pump motor flow speed was estimated with Equation 3 below;

$$\dot{m}_{wf,pump} = \rho V (1 - \sigma) \frac{1425}{3000} f \quad (3)$$

Where ρ is the fluid density at the pump inlet, V is the volume displaced by a single revolution of the pump, f is the frequency of the pump motor (set by the user), $\frac{1425}{3000}$ is the expected pump shaft/electric frequency ratio, and σ is the motor slip factor. See Section 5.1 of this paper for a further investigation into this measurement technique and the motor slip factor.

Energy balances on the condenser and evaporator were used to calculate additional estimates of the working fluid mass flow rate using Equations 4a and 4b;

$$\dot{m}_{wf,evap} = \frac{(\dot{m}\Delta h)_{oil}}{\Delta h_{wf}}, \quad \dot{m}_{wf,cond} = \frac{(\dot{m}\Delta h)_{water}}{\Delta h_{wf}} \quad (4a,b)$$

The $\dot{m}_{wf,cond}$ result is assumed to be more accurate overall, as the water flow rate was measured directly, the water enthalpy of water is well known (as opposed to the thermal oil), and the condenser temperature was closer to ambient, resulting in less ambient heat loss.

A bypass line is included line around the expander to allow the system to heat up and build up pressure without spinning the generator. Additional valves are included in the system to isolate components in case of a leak and for the charging process (Figure 2).

The M1 fluid mixture consists of a zeotropic mixture of R245fa and R365mfc at 52.8% and 47.2% mole fractions. All state properties of the M1 fluid mixture are calculated using the NIST REFPROP 9.0 fluid property database software (Lemmon, 2013).

2.5 Cooling system

The municipal water supply is passed through the condenser in a once-through cooling system. The flow rate is controlled with a gate valve.

2.6 Componentry summary

Table 1: Summary of key components in 1 kW experimental ORC-B system.

COMPONENT	TYPE
Evaporator	Brazed 316 SS plate. 6.374 m^2 total surface area.
Condenser	Brazed 316 SS plate. 1.805 m^2 total surface area.
Thermal oil pump	Gear type pump. 11 cc/rev.
Thermal oil pump motor	1.5 HP (1.1 kW). 1 winding.
Working fluid pump	3 cylinder piston pump. 4.81 cc/rev.
Working fluid pump motor	0.5 HP (373 W). 4 poles.
Expander	Scroll type 12 cc/rev. Fixed volume ratio = 3.5.
Generator	AC asynchronous with voltage regulation. 2.4 kW, 240V operation at 50 Hz.
Working fluid	9.59kg of M1 refrigerant. 50.3 wt% R245fa, 49.7 wt% R365mfc.
Heat transfer fluid	High temperature, low visc. HTF.
DAQ	Compact DAQ.

Table 2: Measurement devices used to determine fluid properties and generator power output. All measurements were recorded at 0.1 Hz.

	Measurement device / method	No.
Exhaust Gas		
Flow	Estimated using manufacturer data.	1
Temperature	Type-K thermocouples.	2
Pressure	Reasonable estimate.	0
Heat Transfer Fluid		
Flow	Gear-pump motor speed. (Equation 2)	1
Temperature	Type-T thermocouples.	2
Pressure	Bourdon tube gauge. Values were not recorded during experiment.	2
Working Fluid		
Flow	Pump motor speed and energy balances (See section 2.4).	3
Temperature	Type-K thermocouples.	4
Pressure	Pressure transducers.	4
Cooling Water		
Flow	Rotary piston meter.	1
Temperature	Type-T thermocouples.	2
Pressure	Estimated from municipal.	0
Power output		
Magnitude & Frequency	Clamp-on power quality meter	1

2.7 Commissioning and charge calculation

9.59 kg or refrigerant change was added to the system through a port situated between the condenser and the buffer tank. The quantity of charge was determined by assuming that the condenser and evaporator should be 30% full of liquid. The piping from the condenser to the evaporator, the pump, and the buffer tank were all assumed to be 100% full of liquid. The experimental results show that this charge amount consistently led to around 10°C of sub-cooling at the condenser exit.

A LABVIEW program created by Alexandre Mugnier is used to sort the data obtained by the DAQ and control the system pump speeds.

Figure 3: Picture of completed test rig at UC.

3. EXPERIMENT

On the 21st February 2014, an experimental run of the ORC-B was performed at a variety of part-load conditions, as outlined in Table 3.

The Capstone turbine was run at a half output setting of 15 kW. The system was run at several refrigerant flow rates for each of the four levels of generator resistances tested as described in Table 3. Each flow rate was maintained for five minutes, or until the system reached steady state.

'Steady state' is defined for the experiment as when the two criteria in Equations 5 and 6 are met;

$$Steady\ state = \sum \frac{|\Delta T_{1-4}|}{\Delta t} < \pm 1\% \quad (5)$$

Where $\Delta t = 30\ seconds$ and T_{1-4} represents the four thermocouple measurements of the working fluid.

$$Steady\ state = \sum \frac{|P_{1-4}|}{\Delta t} < \pm 10\% \quad (6)$$

The pressure criterion excludes single outlier values (+/- > 20 kPa from the average of the previous and subsequent 10 seconds). This additional requirement was included as the pressure measurements are prone to occasional sudden spikes, especially at the high pressure side of the system.

Table 3: User controlled variables during experiment.

COMPONENT	SETTING
Capstone Turbine (heat source)	15 kW Capstone turbine output (270-272 °C exhaust gas temperature, 0.22 kg/s air flow rate)
Thermal Oil Pump	14 Hz (Flow rate 0.12 kg/s dependent on temperature)
Working fluid pump	16 – 21 Hz (Flow rate 0.04 to 0.06 kg/s). Pump motor speed increased in 1 Hz increments every 5 minutes.
Cooling water flow	Inlet valve fully open, flow rate between 0.9 and 1.1 kg/s.
Generator resistance	Bank of light bulbs in parallel with approximately 576 ohms of resistance per bulb when hot (100 W at 240 V). Bulbs added in increments after all tested pump speeds were run for five minutes.

4. RESULTS

Figure 4 shows the refrigerant temperatures during the course of the experiment. The points in time when the pump speed and the generator resistance are changed are indicated. Darker line colours indicate when the steady state criterions were met. Figure 4 indicates that for a given pump speed, increasing the generator resistance resulted in a higher expander outlet temperature.

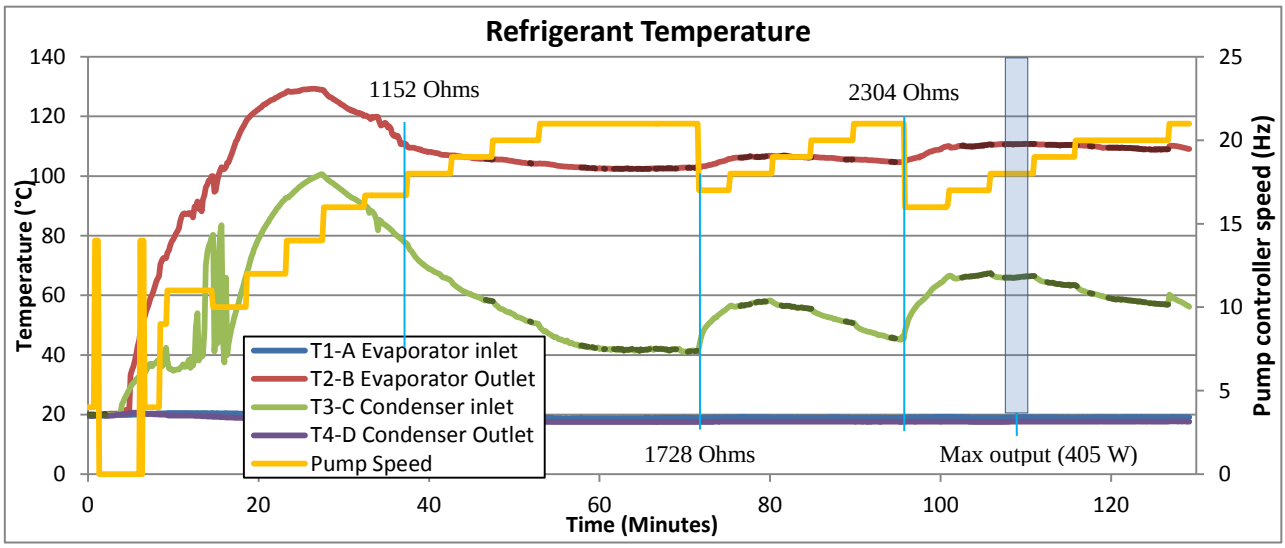

Figure 4: Temperature of refrigerant during the evolution of the experiment. Instances when more resistance was added onto the generator are indicated. Darker areas indicate when the steady state conditions were met.

Table 4: Operating conditions during maximum turbine output at 'relative steady state'. These values are evaluated with the average experiment values between 107 and 110 minutes, indicated by the blue zone in Figure 4.

Position	Temperature (°C)	Pressure (kPa)	Flow rate (kg/s)
Exhaust gas			
FTHE inlet	271.6 ±1.5	(102)	0.22*
FTHE outlet	201.5 ±1.5	(101.3)	-
Thermal oil			
FTHE inlet	86.7 ±1.5	(200)	0.119 ±0.011
FTHE outlet	133.4 ±1.5	191.8*	-
Cooling water			
Condenser inlet	17.3 ±0.5	(200)	1.016 ±0.015
Condenser outlet	20.0 ±0.5	193.8*	-
Refrigerant			
Evaporator outlet	110.7 ±1.5	941 ±28	-
Expander inlet	(110.3)	(941)	-
Condenser inlet	66.0 ±1.5	129 ±14	-
In cond. (sat. vap)	34.2	129.4**	-
In cond. (sat. liq)	28.3	129.4**	-
Condenser outlet	17.6 ±1.5	129 ±14	-
Pump outlet	19.1 ±1.5	946 ±28	(0.0484)
In evap. (sat. liq)	98.0	946.1**	-
In evap. (sat. vap)	102.8	946.1**	-

( ) represents estimated values; * indicates that values are predicted using manufacturer data; ** indicates the data were estimated with the refrigerant state using REFPROP software.

4.2 Net power and efficiency

The cycle thermal efficiency was calculated for the operating conditions between 107 and 110 minutes from Table 4, as additional surface temperature measurements were taken during this time (Section 5.3). The average gross power output measured by the clamp meter for this time period was 405 ±10 W. The working fluid pump electrical input power was not measured, and so it is estimated using Equation 7.

$$W_{in,wf\ pump} = \frac{m(h_{pump\ outlet} - h_{condenser\ outlet})}{\eta_{pump\ and\ motor}} \quad (7)$$

Where; $h_{pump\ outlet}$ and $h_{condenser\ outlet}$ are the enthalpies of the M1 fluid at both sides of the pump, calculated using the REFPROP property database and the measured temperature and pressure values. $\eta_{pump\ and\ motor}$, the efficiency of conversion from electrical input energy to the fluid, is assumed to be 80%.

Using Equation 7, the estimated working fluid pump power is 140 W.

The thermal oil gear pump input power was not measured during the experiment. The gear pump motor power is assumed to be negligible due to the small pressure drop across the heat exchangers (Table 4).

The estimated net power output from the experiment ($W_{net} = W_{gross} - W_{in}$) is 265 W.

The overall thermal efficiency of the cycle during this experiment is;

$$\eta_{th} = \frac{W_{net}}{Q_{in}} = \frac{0.265}{13.2} = 2.01\% \pm 0.99\%. \quad (8)$$

It should be noted that higher thermal efficiencies than the above value have been observed when the ORC-B system is run at other operating conditions.

For comparison, the maximum theoretical triangular cycle efficiency within the available temperatures is;

$$\eta_{tri} = \frac{T_H - T_L}{T_H + T_L} = \frac{406.5 - 290.4}{406.5 + 290.4} = 16.66\% \quad (9)$$

And the maximum possible cycle efficiency is approximately (Invernizzi, 2013);

$$\eta_{max} \approx 1 - \frac{T_{Condensation}}{T_{H,Average}} = 1 - \frac{303.35\ (K)}{383.2\ (K)} = 19.79\% \quad (10)$$

The second law efficiency is thereby approximately;

$$\frac{\eta_{th}}{\eta_{max}} \approx \frac{2.01\%}{19.79\%} = 10.2\ \% \quad (11)$$

This low value of the second law efficiency indicates that there is significant room for improvement in plant sophistication, as small scale ORCs can be expected to provide second law efficiencies as high as 50% (Invernizzi, 2013). It can be expected that the ORC-B will achieve greater second law efficiencies when operated closer to its design conditions.

5. OBSERVATIONS AND POTENTIAL SOURCES OF ERROR

5.1 Working fluid pump motor slip

The motor slip factor is a commonly used variable to represent the slip that occurs between a motor and a shaft (Equation 3).

The motor slip factor was estimated using Equation (12)

$$\sigma \approx \frac{\dot{m}_{wf,pump'} - \dot{m}_{wf,cond}}{\dot{m}_{wf,pump'}} \quad (12)$$

Where $\dot{m}_{wf,pump'}$ is the estimated mass flow rate of refrigerant using Equation (3) if $\sigma = 0$.

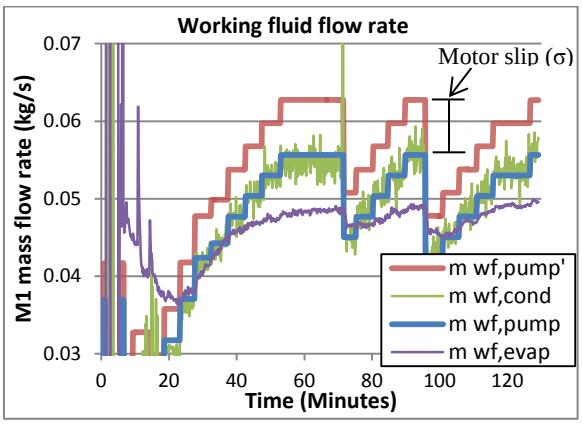

Figure 5: Flow rate as measured by pump speed with and without slip factor (σ = 0.113) correction.

The average motor slip value for the system was calculated from the steady state experimental results (Figure 4). The resulting average motor slip value was $\sigma \approx 0.113$ (Figure 5). This value is somewhat larger than the commonly assumed value for small pump motors of 0.05 (Peltola, 2002), and may indicate leakage in the pump cylinders or the presence of vapour bubbles entrained in the pump inlet flow (Quoilin, 2007).

5.2 Ball valve pressure drop

A further experiment was conducted on the same system on the 30th January 2014 with the objective of comparing the change in system performance after a restrictive ball valve was replaced. Detailed results for the system with the restrictive ball valve had already been obtained, and are detailed in (Jung, 2014, in progress).

The ball valve was situated about 150 mm before the expander inlet. It had been suspected that the geometry of the ball valve may have contributed to a significant unmeasured pressure drop before the flow entered the expander (Jung, 2014, in progress).

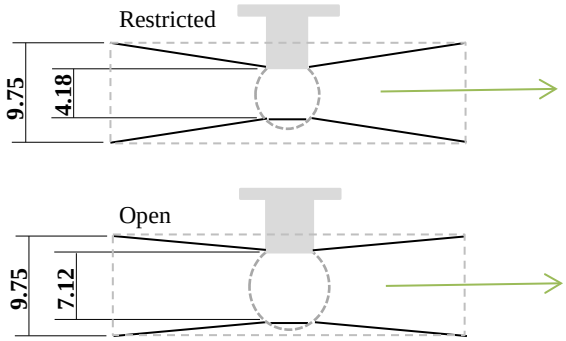

Figure 6a and b: Geometry of old (top) and new (bottom) ball valves situated just before the expander inlet. All dimensions are in mm (Swagelok, 2013).

The original 'restricted' ball valve (Figure 6a) was a model SS-43GS8 Swagelok part from Swagelok New Zealand. It was replaced with a new part, SS-AFSS8 before the experiments in this report were undertaken.

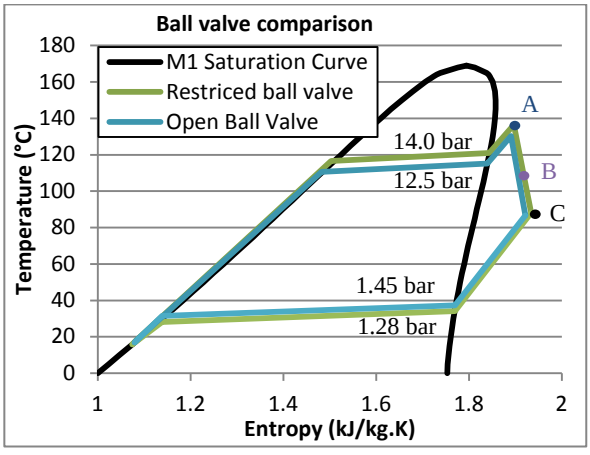

Figure 7: T-s diagram of refrigerant flow under identical operating conditions before and after ball valve replacement. State A represents to measurements at the evaporator exit. State B is the theoretical state at the expander inlet and state C is the measured state at the condenser inlet.

Data from manufacturer testing was consulted during the ORC build. This data, produced from tests with water, indicated that the 'restricted' valve could be expected to result in a pressure drop of up to 5 bar at the higher flow rates used by the ORC system (Swagelok, 2013).

Figure 7 shows a T-s diagram for the system before and after the ball valve was replaced. The operating conditions are identical except from a small change in condenser water and ambient temperature.

For ease of analysis, and because of its small effect on the result, it can be assumed that all the work is extracted at the end of the expansion process. This work extraction is then represented by the flow from state B to state C in Figure 7. The theoretical power output of the turbine can then be calculated with Equation 13.

$$\dot{W}_{out,theory} = \eta_{Gen.and\ Bearings} \times \dot{m}_{wf,turb}(h_B - h_C) \quad (13)$$

Where; $\dot{m}_{wf,turb}$ is the mass flow rate through the turbine (excluding leakage) calculated using the measured speed of the generator with an estimated slip of 0.05, and the known volumetric capacity of the expander, h_B is the enthalpy of the refrigerant before it has undergone an expansion with a volumetric ratio of 3.5, and h_C is the enthalpy of the refrigerant at state C. $\eta_{Gen.and\ Bearings}$ accounts for the combined efficiency of the magnetic shaft coupling and generator, assumed to be 90%.

In the 'restricted' ball valve scenario, the measured system power output is 405 W, while the theoretical power output due to the enthalpy loss between states B and C is 721 W. In the 'new ball valve' scenario, the measured output power totaled 553 W, while the theoretical power output is 643 W. This difference between the measured and theoretical power output under identical operating conditions was used to determine the effect of the restricted ball valve.

$$\dot{W}_{out,unexplained} = \dot{W}_{out,theory} - \dot{W}_{out,measured} \quad (14)$$

The 'restricted' ball valve test had an unexplained power loss of 316 W while the 'open' ball valve only has a 90 W loss when compared to the theoretical output. If the additional 226 W of lost power of the 'restricted' ball valve test (W_{lost}) is assumed to be due to a pressure drop across the restricted ball valve, then the minimum magnitude of the pressure loss can be estimated. Using the average isentropic efficiency of the expansion process η_{isen} of 72.6%, the expected expander inlet enthalpy if there were no pressure loss can be estimated for the 'restricted' ball valve scenario;

$$h_{no\ loss} = h_{B,restricted} + \frac{W_{lost}}{\dot{m}_{wf}.\eta_{isen}} \quad (15)$$

Where; $h_{no\ loss}$ is the estimated scroll inlet enthalpy if there was no pressure loss from the ball valve.

A corresponding minimum inlet pressure was determined by using the calculated entropy at point B and the property database in the REFPROP software.

$$P_{loss} > P_{no\ loss,isen} - P_B = 130\ kPa \quad (16)$$

The estimated minimum pressure drop across the restricted ball valve, P_{loss}, is 1.30 bar.

5.3 Heat loss

Surface temperature measurements of the hot components in the cycle were taken during operation at the conditions described in Table 4. Preliminary 1-dimensional heat loss calculations were used to estimate the magnitude of any effect of ambient heat losses. Nussult number correlations as found in (Theodore L. Bergman, 2011) were used to estimate convection coefficients. A summary of the average surface temperatures and estimated heat loss is given in Table 5.

Table 5: Average surface temperature measurements and estimated heat loss.

Component	Exposed surface area (m^2)	Average surface temp. (°C)	Conv. heat loss (W)	Rad. heat loss (W)
Evaporator	0.504	80	122.2	89.6
Expander	0.063	68	11.4	2.3
Piping 1*	0.022	92	17.2	3.9
Piping 2*	0.048	51	12.9	2.8
Total	**0.637**		**262.3**	

*Piping 1 represents the section of pipe between the evaporator and expander. Piping 2 represents the section between the expander and condenser.

The estimated heat loss from the 'Piping 1' section indicates that the expander inlet temperature is 0.35°C lower than what is recorded at the evaporator outlet in Table 4.

The total estimated heat loss between the evaporator outlet and the condenser inlet is the equivalent of about 0.93°C of refrigerant temperature. This heat loss reduces the entropy of the measured condenser inlet condition (point C in Figure 7). This indicates an isentropic efficiency of the expansion process in the ball valve test of 2.03 % lower in reality than what is calculated from existing temperature measurements.

The total estimated heat loss from the uninsulated hot pipes, evaporator and expander is 262.3 W, or up to 2.0% of Q_{in}, the overall total heat input in Equation 8.

5.4 Measurement error

Table 6: Error of measurement devices as specified by their respective manufacturers.

Component	Error
Thermocouples	K-type ±1.5°C, T-type ±0.5°C
Pressure transducers	LP ±14 kPa, HP ±28 kPa
Clamp meter	2.5% of measured value
Water flow meter	1.5% of measured value

5.5 Analytical sources of error

The property information contained in the REFPROP database contains an unknown level of inaccuracy for some fluids (DiPippo & Moya, 2013). This is applicable to the M1 mixture used as the mixing parameters were estimated.

The heat capacity formula used for the thermal oil (Equation 1) is likely to be inaccurate, as a heat balance on the evaporator often indicates a negative ambient heat loss when using the current equation, even when considerable (σ = 0.05) motor slip on the gear pump is assumed. This is evidenced by the consistent underestimate of M1 flow rate in Figure 5, produced from using the evaporator heat balance described in Equation 4a.

5.6 Error analysis on efficiency calculation

An error propagation analysis including both the measurement error and potential heat loss indicates that the total accounted relative error of the measured net thermal efficiency value is ±1.0%, as shown in Equation 8. A large portion of this error (±0.8%) is attributable to the potentially much higher or lower work input to the pump than Equation 7 suggests, due to the accuracy of the thermocouples. Direct measurement of the working fluid pump motor power is recommended to overcome this limitation.

Further experimentation is necessary before the magnitude of any potential inaccuracies in the M1 and thermal oil property information can be estimated.

6. CONCLUSION

An experimental ORC test bench designed to operate at 1 kW was run at the University of Canterbury at partial load conditions. Steady state experimental results were obtained and analysed in order to gain insight into ORC system behaviour. The thermal efficiency of the system at this operating condition was found to be $2.01\% \pm 0.99\%$ and the second law efficiency approximately 11.0%.

Ways in which the complex interaction of components in an ORC can conflate measurements and produce unexpected experimental results were investigated, and specific components were analysed for their behaviour. The working fluid pump motor was found to have a slip coefficient of $\sigma \approx 0.11$. The previously installed restrictive ball valve was found to have a minimum pressure drop of $P_{loss} > 130\ kPa$. The system heat loss was found to be in the order of 260 W and component measurement error was found to add nearly a 1% uncertainty onto the system thermal efficiency calculation.

While these known results have been obtained from running the system, several unknown factors such as the exact thermodynamic properties of the thermal oil and working fluid affect the outcome of the investigations in this paper. Additional improvements to the ORC-B system and further experimentation designed to analyse these properties would be required in order to reduce the potential error of results obtained from the system.

7. FUTURE WORK

As a result of the analysis in this paper, additional measuring equipment has been added to the system since the described experiments took place, and new experiments are due to start in September 2014. These improvements include;

Two clamp meters to measure the power of the working fluid pump and the thermal oil pump, insulation on the evaporator and hot pipes, a variable area flow meter suitable for measuring the refrigerant flow rate, and both pressure transducers and thermocouples placed shortly before and after the expander inlet and outlet respectively. The additional thermocouples and pressure transducers have been added to more accurately measure the expander flow conditions and any pressure drop due to the remaining valve restriction.

Additional testing with the new instrumentation to better determine the heat capacity of thermal oil and the M1 fluid is also set to be undertaken.

ACKNOWLEDGEMENTS

This work was supported by the New Zealand Heavy Engineering Research Association funded by Ministry for Science & Innovation.

The setup of the test rig and experiments for this work were conducted with Alexandre Mugnier, Deborah Forveil and Damien Ronchetti. Extra thanks to Alexandre for preparing the LABVIEW operation and recording program.

Preliminary analysis of the results and heat loss calculations were conducted with the help of Valentin Dubois.

The author would like to thank the ORC research team at the University of Canterbury for their helpful feedback and ideas. The author would also like to thank Dr. Susan Krumdieck and Dr. Mark Jermy of the University of Canterbury for their continued support and direction.

REFERENCES

Capstone, Turbine Corporation. (2006). Technical Reference Capstone Model C30 (Vol. Rev. D, pp. 35,55,57).

David Meyer, Choon Wong, Frithjof Engel, Susan Krumdieck. (2013). *Design and build of a 1 kW organic rankine cycle power generator* Paper presented at the 35th New Zealand Geothermal Workshop, Rotorua, New Zealand.

DiPippo, Ronald, & Moya, Paul. (2013). Las Pailas geothermal binary power plant, Rincón de la Vieja, Costa Rica: Performance assessment of plant and alternatives. *Geothermics*, *48*(0), 1-15. doi: http://dx.doi.org/10.1016/j.geothermics.2013.03.006

Engel, Frithjof. (2013). *Experiemental Investigation and Derived Considerations for the Scale-Up of a Finned-Tube Heat Exchanger for Exhause Gas Heat Recovery.* (MSc Master's Thesis), Hamburg University of Technology.

Invernizzi, Mario. (2013). *Closed Power Cycles: Thermodynamic fundamentals and applications* (Vol. 11). London: Springer.

Jung, H. C., Leighton Taylor, Susan Krumdieck. (2014, in progress). An experimental and modelling study of a 1 kW organic Rankine cycle with mixture working fluid. *Energy*.

Lemmon, E.W., McLinden, M.O., Huber, M.L. (2013). REFPROP-Reference Fluid Thermodynamic and Transport Properties (Version 9.0): NIST NSRDS.

Lemort, Vincent, Quoilin, Sylvain, Cuevas, Cristian, & Lebrun, Jean. (2009). Testing and modeling a scroll expander integrated into an Organic Rankine Cycle. *Applied Thermal Engineering*, *29*(14–15), 3094-3102. doi: http://dx.doi.org/10.1016/j.applthermaleng.2009.04.013

Peltola, Mauri. (2002, 11/15/2002). AC induction motor slip. *PlantServices*, 2.

Quoilin, Sylvain. (2007). *Experimental Study and Modeling of a Low Temperature Rankine Cycle for Small Scale Cogeneration.* (Electro-Mechanical Engineeer), University of Liege.

Swagelok. (2013). One-Piece Instrumentation Ball Valves. In S. USA (Ed.), *40G Series and 40 Series* (pp. 12).

Theodore L. Bergman, Adrienne S. Lavine, Frank P. Incropera, David P. DeWitt. (2011). *Fundamentals of Heat and Mass Transfe* (7th ed.): Wiley.